Journal of Solid State Chemistry **144,** 379–387 (1999)
Article ID jssc.1999.8169, available online at http://www.idealibrary.com on IDEAL®

Structural Study of Modified $Bi_4V_2O_{10+\delta}$ Phases ($\delta = 0, 0.5, 1$): Influence of Antimony Contribution

S. Sorokina,* R. Enjalbert,*,[1] P. Baules,* A. Castro,† and J. Galy*

*Centre d'Elaboration de Matériaux et d'Etudes Structurales, CNRS, 29 rue Jeanne Marvig, B.P. 4347, 31055 Toulouse Cedex 4, France; and †Instituto de Ciencia de Materiales de Madrid, CSIC, Cantoblanco, 28049, Madrid, Spain

Received October 7, 1998; in revised form December 24, 1998; accepted January 10, 1999

Three solid solutions of general composition $Bi_{4-x}Sb_xV_2O_{10}$, $Bi_4V_{2-y}^{4+}V_y^{5+}O_{10+y/2}$, and $Bi_4V_{2-z}Sb_zO_{11}$ have been investigated in the fivefold Bi_2O_3–V_2O_5–V_2O_4–Sb_2O_3–Sb_2O_5 system. These oxides have been characterized by X-ray diffraction and electron microscopy techniques. Single phases have been isolated for values ranging from 0 to x, $z = 0.8$ and $y = 2$. Single crystals of $Bi_{3.2}Sb_{0.8}V_2O_{10}$, $Bi_4V_2O_{10.5}$, and $Bi_4V_{1.2}Sb_{0.8}O_{11}$ have been grown and their structures determined by X-ray diffraction methods. The three oxides crystallize in the orthorhombic system, space groups F222, Amam, and Fmmm, respectively. Their structures keep the classical two-dimensional array of Aurivillius-like oxides with (Bi, Sb)–O layers interleaved with (V, Sb)–O sheets. It has been found that Sb^{3+} is introduced into the bismuth layer, due to its similar sterical behavior, by the presence of a $5s^2$ lone pair associated with Sb^{3+} and $6s^2$ associated with Bi^{3+}, whereas Sb^{5+} substitutes for the V^{5+} cation. All of the substitutions carried out mainly act on the vanadium layer, which can accommodate different coordination polyhedra for cations: tetrahedra for V^{5+}, square pyramids and distorted trigonal bipyramids or octahedra for V^{4+} and V^{5+}, and octahedra for Sb^{5+} . This fact can be related to the electrical properties, such as high ionic conduction and ferroelectricity, shown by these types of materials.

INTRODUCTION

The bismuth vanadium mixed oxide $Bi_4V_2O_{11}$ has attracted a lot of attention as the parent phase for a family of oxide-ion conductors known as BIMEVOX (1–4) that exhibits interesting oxygen conductivity at low temperature. For example, Cu-substituted $Bi_4V_2O_{11}$ (BICUVOX) is one of the best oxide-ion conductors possessing an oxide-ion transference number near unity at atmosphere P_{O_2} (1). $Bi_4V_2O_{11}$ was first identified in the binary system Bi_2O_3–V_2O_5 (5). Its structure is closely related to the simplest $n = 1$ Aurivillius phases with alternating $[Bi_2O_2]_n$ and $[VO_{3.5}]_n$ layers, and it undergoes two structural transitions upon on heating ($\alpha \rightarrow \beta \rightarrow \gamma$) before melting, as confirmed by several techniques (6). Both room temperature α and β phases seem to crystallize in the orthorhombic system with ordered oxygen vacancies, while at high temperatures the γ phase becomes a disordered structure leading to a tetragonal cell and appreciably higher conductivity.

To stabilize the high-temperature disordered phase, a classical chemical way of substituting other cations for V^{5+} was carried out to prevent ordering of the structure. These substitutions were successfully realized with a large variety of metallic cations and led to the above-mentioned BIMEVOX family. If V^{5+} is partly replaced by the isovalent cation Sb^{5+}, different structural modifications can be detected in the system $Bi_4V_{2-x}Sb_xO_{11}$ as a function of the composition. Some authors (7) claimed the existence of an α phase up to $x = 0.15$ and the β phase between 0.15 and 0.30 beyond this limit; the γ phase is characterized up to $x = 1.0$. These authors reported very good ionic-conducting properties for the phases with 0.20 to 0.30 antimony content. Other authors reported the existence of a solid solution of general composition $Bi_4V_{2-y}Sb_yO_{11-\delta}$ ($0 \leq y \leq 0.3$) and studied the catalytic behavior of these materials (8). Joubert *et al.* (9) determined the crystal structure of a mixed V^{4+}/Sb^{5+} doped phase $Bi_4V_{1.5}Sb_{0.5}O_{10.7}$, which is an electronic insulator at room temperature.

On the other hand, the existence of the solid solution $Bi_4V_{2-z}^{5+}V_z^{4+}O_{11-z/2}$ by substitution of V^{4+} for V^{5+} in the parent structure $Bi_4V_2O_{11}$, keeping the Aurivillius framework, was evidenced (10). The limiting oxide $Bi_4V_2O_{10}$ also exhibits three polymorphic phases on heating, α, β, and γ, with the orthorhombic symmetry and decreasing vacancy ordering as in $Bi_4V_2O_{11}$ (11). This material is a very good ionic conductor with a conductivity as high as $10^{-1}\,\Omega\,cm^{-1}$ at 730°C (12). Moreover, other lone pair cations, such as Sn^{2+}, Sb^{3+}, or Te^{4+}, can be substituted in the $[Bi_2O_2]_n$ layer of the Aurivillius structure (13–15) or, in the particular case of $n = 1$ Aurivillius-like phases, Bi^{3+} can be completely replaced by Sb^{3+} (16–18).

[1] To whom correspondence should be addressed.

0022-4596/99 $30.00

The different cation substitutions in both $[Bi_2O_2]_n$ and $[A_{n-1}B_nO_{3n+1}]_n$ layers of the Aurivillius-type structures have a strong influence on the crystal structures of these oxides and therefore on their physical properties. Antimony introduction into the $Bi_4V_2O_{11-\delta}$ framework could be interesting for two reasons: (i) Sb^{3+} has a $5s^2$ stereo chemically active lone pair of electrons, like the $6s^2$ of Bi^{3+}; and (ii) Sb can exhibit two oxidation states, Sb^{3+} and Sb^{5+}, occupying both bismuth and/or vanadium positions, respectively. This paper reports results on the solid solutions appearing in the Bi_2O_3–V_2O_5–V_2O_4–Sb_2O_3–Sb_2O_5 system.

EXPERIMENTAL

Synthesis

Powdered samples were prepared by solid-state reactions from ground stoichiometric mixtures of analytical grade Bi_2O_3, VO_2 and/or V_2O_5, and Sb_2O_3 or Sb_2O_5 oxides. VO_2 was prepared by heating an equimolar mixture of V_2O_5 and V_2O_3 at 850°C for 3 days. V_2O_3 itself was obtained by reducing V_2O_5 under hydrogen at 800°C for 12 h. All reactions from V_2O_3, VO_2, and Sb_2O_3 were carried out in sealed evacuated quartz tubes to prevent any oxidation. The samples were heated for 24 h at final temperatures of 650°C for Bi_2O_3, VO_2, and Sb_2O_3 starting oxides and 850°C for the remaining samples. After the thermal treatment, the products were quenched to room temperature and characterized by X-ray powder diffraction.

Single crystals of representative compositions were grown from melted stoichiometric mixtures of starting oxides. The mixtures were placed into ampoules sealed under vacuum or in platinum boats for treatment under O_2; similar reactions were made to obtain polycrystalline samples. They were heated at 950°C except for $Bi_2O_3 + VO_2 + Sb_2O_3$ reactions, which melted at 850°C. They were cooled down to 400°C at 5°C h^{-1} and to room temperature at 50°C h^{-1}. This protocol results in the formation of black (for V^{4+}) or dark brown (for V^{5+}) platelet crystals of adequate size (width and length, from 0.1 to 1 mm; thickness, around 0.02 mm) to be studied by X-ray single crystal diffraction methods.

X-ray Diffraction

Powder X-ray diffraction patterns were recorded with graphite monochromatized Cu$K\alpha$ radiation and a Seifert XRD 3000 diffractometer scanning from 4° to 64° (2Θ) in steps of 0.05° (2Θ) and with 3 s counting time at each step. The unit-cell parameters derived from X-ray powder data were refined through least-squares techniques.

The single-crystal quality and the crystal systems were first investigated on a precession camera. The diffraction data were collected with an Enraf-Nonius CAD4 diffractometer. Orientation matrix and cell parameters were obtained from least-squares refinements of the setting angles of 25 *hkl* reflections. Corrections for Lorentz polarization and empirical absorption (19) were applied to the data. Atomic scattering factors were corrected for anomalous dispersion (20). The calculations were performed with SHELX-86 (21) and the drawings with ORTEP (22).

Electron Microscopy

The transmission electron microscopy (TEM) experiments were performed on ground single crystals with a Philips CM20 electron microscope working at an accelerating voltage of 200 kV. This microscope is equipped with an EDX system permitting the verification of the presence of the expected elements in each studied region.

RESULTS AND DISCUSSION

To verify the possibility of substitution of Sb^{3+} for Bi^{3+} in the bismuth layer and of V^{4+} or Sb^{5+} for V^{5+} in the vanadium layer of $Bi_4V_2O_{11}$ $([Bi_2O_2][VO_{3.5}])_2$, three solid solutions were investigated in the fivefold system Bi_2O_3–V_2O_5–V_2O_4–Sb_2O_3–Sb_2O_5 shown in Fig. 1: (I) $Bi_{4-x}Sb_xV_2O_{10}$ ($x \leq 0.8$), (II) $Bi_4V_{2-y}^{4+}V_y^{5+}O_{10+y/2}$ ($0 \leq y \leq 2$), and (III) $Bi_4V_{2-z}Sb_zO_{11}$ ($z \leq 0.8$).

Type I: Solid Solution $Bi_{4-x}Sb_xV_2O_{10}$ ($x \leq 0.8$)

X-ray diffraction patterns of representative samples belonging to this solid solution are shown in Fig. 2. In the range $0 \leq x \leq 0.8$ the samples show the evolution of a nonstoichiometric single phase while slightly polluted by a tiny bit of $SbVO_4$ and Sb_2VO_5 for $x = 0.6$ and $x = 0.8$ respectively. The patterns were indexed by taking the γ-$Bi_4V_2O_{10}$ compound as a structural model (11). The evolution of the

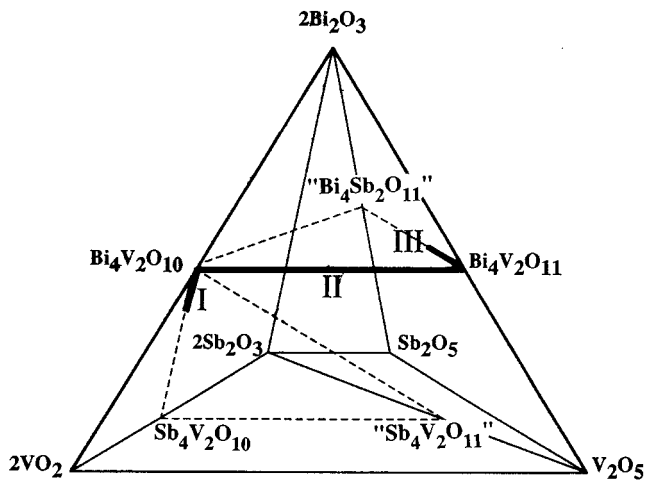

FIG. 1. Solid solutions studied in the schematic fivefold diagram Bi_2O_3–V_2O_5–V_2O_4–Sb_2O_3–Sb_2O_5.

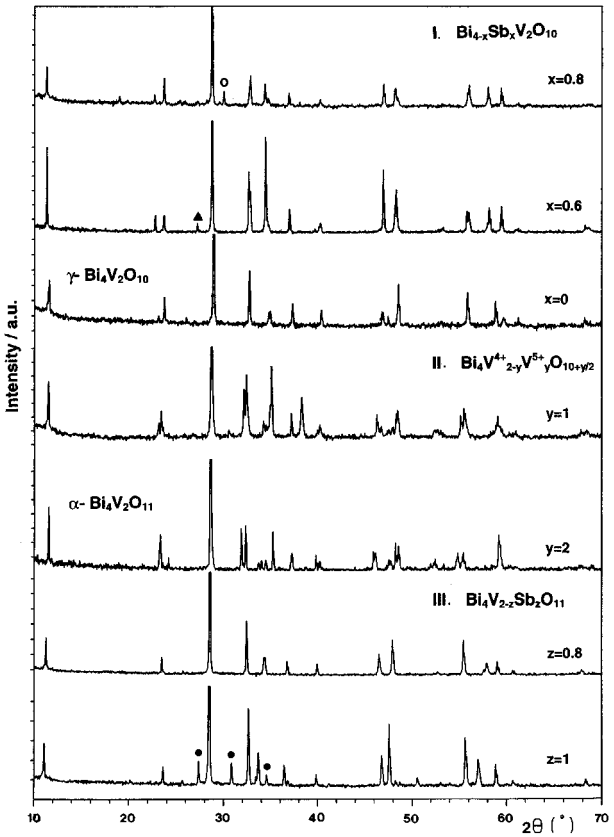

FIG. 2. X-ray diffraction patterns of representative samples in the solid solutions (I) $Bi_{4-x}Sb_xV_2O_{10}$, (II) $Bi_4V_{2-y}^{4+}V_y^{5+}O_{10+y/2}$, and (III) $Bi_4V_{2-z}Sb_zO_{11}$. (○, Sb_2VO_5; ▲, $SbVO_4$; ●, $BiSbO_4$) .

mean unit-cell parameters is depicted in Fig. 3I. The lattice parameter b decreases while c increases with increasing Sb^{3+} content up to about $x = 0.8$. Subsequently, the parameters remain unchanged for higher values so the maximum limit of x to yield the solid solution is found to be 0.8.

To understand the structural evolution in the $Bi_{4-x}Sb_xV_2O_{10}$ solid solution, single crystals of the limiting composition $x = 0.8$, $Bi_{3.2}Sb_{0.8}V_2O_{10}$, were grown. An initial study was made by electron diffraction (ED) and TEM. The electron diffraction patterns (Fig. 4I) do not reveal the presence of superlattice spots, which are a characteristic feature of the undoped γ-$Bi_4V_2O_{10}$ phase (11).

The structure of $Bi_{3.2}Sb_{0.8}V_2O_{10}$ has been determined by single-crystal diffraction methods. Table 1 summarizes physical and crystallographic data together with the conditions of data collection. The atomic parameters are listed in Table 2 and selected distances are shown in Table 3.

The framework of this structure keeps the classical arrangement of Aurivillius-like $n = 1$ phases (Fig. 5), being built up by $[Bi_{1.6}Sb_{0.4}O_2]_n$ sheets interleaved with $[V_2O_6]_n$ layers, which contain VO_5 square pyramids sharing their basal corners.

The antimony and bismuth atoms occupy statistically two very close crystallographic sites (0.27 Å) in the network. Both atoms are coordinated to four oxygens (two O1 and two O2) of its layer, at shorter distances for antimony than bismuth (Table 3) according to its smallert ionic radii (23).

Despite this Sb–O shortening, the c parameter of the cell increases; this fact can be explained by the stronger stereoactivity of the Sb^{3+} lone pair. For Bi^{3+} we must also note the tendency of the electronic lone pair to come closer to the nucleus due to relativistic effects. We note that the Sb

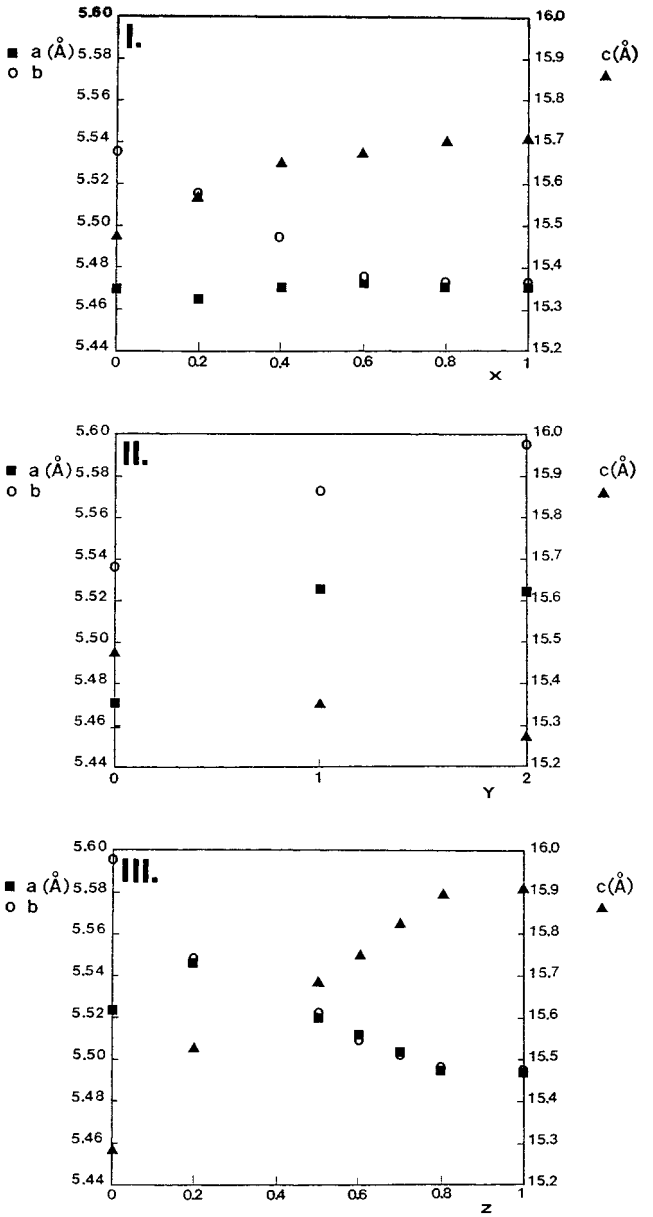

FIG. 3. Evolution of mean unit-cell parameters as a function of doping content in (I) $Bi_{4-x}Sb_xV_2O_{10}$, (II) $Bi_4V_{2-y}^{4+}V_y^{5+}O_{10+y/2}$, and (III) $Bi_4V_{2-z}Sb_zO_{11}$ phases. (On the left, the values concern the a and b cell parameters. On the right, the values concern the c cell parameters).

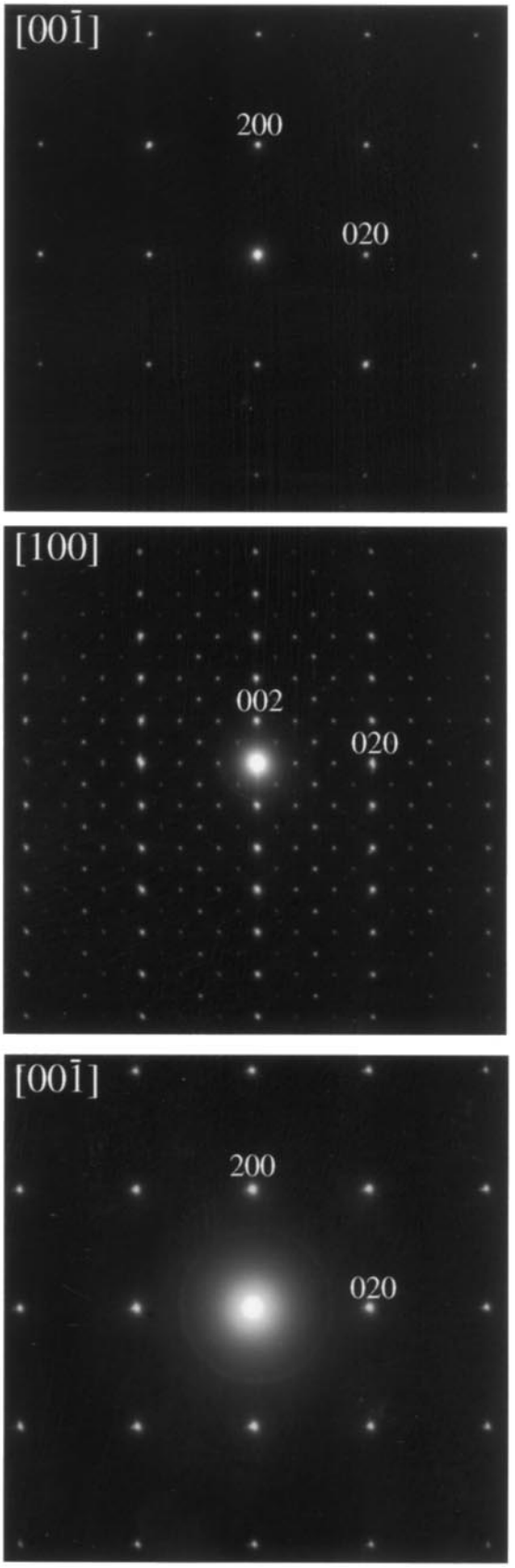

substituting for Bi does not occupy its crystallographic sites, but clearly a different position, highlighting their different stereochemistry behavior.

The $[V_2O_6]_n$ layers exhibit classical disorder; they have difficulty fitting the imposed periodicity of the pavement laid down by the $(Bi,Sb)O_4E$ square pyramids (E symbolizes the lone pair). Two crystallographically independent sites, rather close (0.36 Å and 0.45 Å), welcome the vanadiums, i.e., V1 and V2. The oxygens O3 and O4 are distributed statistically. Nevertheless, the V–O interatomic distances, ranging from 1.67 Å up to 2.23 Å, retain their usual values but show an important distortion of the VO_5 square pyramids.

Type II: Solid Solution $Bi_4V_{2-y}^{4+}V_y^{5+}O_{10+y/2}$ ($0 \le y \le 2$)

The existence of a continuous solid solution between the extensively studied $Bi_4V_2O_{11}$ oxide and the homologous V^{4+}-substituted compound $Bi_4V_2O_{10}$ has been presented by Galy *et al.* (10–11). Here we report the mean structure of the midway oxide $Bi_4V_2O_{10.5}$ ($y = 1$), containing both V^{4+} and V^{5+} cations.

The powdered sample $Bi_4V_2O_{10.5}$ was first characterized by X-ray powder diffraction methods. Its diffraction pattern (Fig. 2) is related to both γ-$Bi_4V_2O_{10}$ and α-$Bi_4V_2O_{11}$ phases and the a, b, and c unit-cell parameters calculated are between those of the limiting phases (Fig. 3II).

As in the type I phases, single crystals were grown to study the original structural features induced by the simultaneous presence of V^{4+} and V^{5+} in the framework. The TEM diffraction pattern (Fig. 4II) clearly exhibits the existence of diffraction maxima corresponding to the existence of superstructure on both b^* and c^* reciprocal axes. This superstructure appears clearly to be commensurate and can be written in the form $b^*/3 + c^*$. This fact shows that 50% substitution of V^{5+} does not stabilize at room temperature the highly ionic conducting γ-phase of either limiting phase $Bi_4V_2O_{11}$ and $Bi_4V_2O_{10}$, which contrasts with other cationic substitutions in the BIMEVOX series. Many examples of γ-type solid solutions stabilized by different metal cations have been reported, mainly dealing with an isovalent cation such as Nb^{5+} or Ta^{5+}, starting from a doping content of about 10% (24, 25) or 15% (7), or an aliovalent cation such as Cu^{2+}, Ni^{2+}, Fe^{3+}, Mn^{4+}, Ti^{4+}, … (see Refs. (6, 26)) and references therein) with an adjusted substitution level according to the metal element, but always lower than 20%. This difference can be related to the limited structural distortion carried out by the introduction of V^{4+} into the V^{5+} framework.

FIG. 4. TEM diffraction patterns of (I) $Bi_{3.2}Sb_{0.8}V_2O_{10}$ with zone axis [00$\bar{1}$], (II) $Bi_4V_2O_{10.5}$ with zone axis [100], and (III) $Bi_4V_{1.2}Sb_{0.8}O_{11}$ with zone axis [00$\bar{1}$].

TABLE 1
Crystallographic Data for $Bi_{3.2}Sb_{0.8}V_2O_{10}$, $Bi_4V_2O_{10.5}$, and $Bi_4V_{1.2}Sb_{0.8}O_{11}$

	Formula		
	$Bi_{3.2}Sb_{0.8}V_2O_{10}$	$Bi_4V_2O_{10.5}$	$Bi_4V_{1.2}Sb_{0.8}O_{11}$
	Crystal data		
Crystal system	Orthorhombic	Orthorhombic	Orthorhombic
Space group	*F*222 (No. 22)	*Amam* (No. 63)	*Fmmm* (No. 69)
a (Å)	5.492(1)	5.527(2)	5.462(2)
b (Å)	5.493(1)	5.574(1)	5.469(2)
c (Å)	15.584(2)	15.351(4)	15.867(4)
V (Å^3)	470.1(2)	472.9(2)	474.0(2)
Z	2	2	2
Molecular weight	1028.0	1015.8	1170.5
ρ calc (g cm^{-3})	7.26	7.13	8.20
μ (Mo$K\alpha$) (cm^{-1})	610.8	725.3	738.7
Morphology	Platelet	Platelet	Platelet
Color	Black	Black	Dark brown
Dimensions (mm)	$0.14 \times 0.12 \times 0.017$	$0.175 \times 0.126 \times 0.021$	$0.138 \times 0.113 \times 0.028$
	Data collection		
Temperature (°C)	20	20	20
Wavelength (Mo$K\alpha$) (Å)	0.71069	0.71069	0.71069
Monochromator	Graphite	Graphite	Graphite
Scan mode	ω–2θ	ω–2θ	ω–2θ
Scan width (°)	$0.90 + 0.35 \tan\theta$	$1.50 + 0.35 \tan\theta$	$1.05 + 0.35 \tan\theta$
Take-off angle (°)	3.2	3.7	3.8
T max (s)	60	60	60
Max Bragg angle (°)	35	35	35
hkl range	$0 \rightarrow 8/0 \rightarrow 8/0 \rightarrow 25$	$0 \rightarrow 8/0 \rightarrow 8/0 \rightarrow 24$	$0 \rightarrow 8/0 \rightarrow 8/0 \rightarrow 25$
	Structure refinement		
Reflections collected	1294	1279	1254
Reflections used	277	398	217
Parameters	23	31	18
R	0.043	0.096	0.120
w	$1/\sigma^2(F) + 0.0019F^2$	1	1
R_w	0.060	0.11	0.144

The structure of $Bi_4V^{4+}V^{5+}O_{10.5}$ was determined by single-crystal diffraction methods. Table 1 summarizes physical and crystallographic data together with the conditions of data collection. The list of fractional coordinates and thermal parameters are given in Table 2. The selected distances are listed in Table 3.

The network of $Bi_4V^{4+}V^{5+}O_{10.5}$ is built up by $[Bi_2O_2]_n$ and $[V^{4+}V^{5+}O_{6.5}]_n$ layers, both V^{4+} and V^{5+} cations making VO_5 square pyramids and V^{5+} cations also VO_4 tetrahedra. These results can be compared with the structural studies for a phase with lower V^{4+}/V^{5+} molecular ratio, $Bi_4V_2O_{10.66}$, carried out by Rietveld refinements using synchrotron radiation powder diffraction data (27) or electron diffraction and high-resolution electron microscopy (28). It appears that this oxide crystallizes in the orthorhombic system space group Pnma with the *b* parameter tripled. Its vanadium–oxygen layer is built up by one $V^{4+}O_6$ octahedron sharing equatorial corners with two $V^{5+}O_4$ tetrahedra. These polyhedra form triple chains infinitely connected along the [100], but not in the [010] direction, breaking the infinite two-dimensional character of that layer in Aurivillius-related phases. An increase of V^{4+} content, like the compound presented here, would allow recovery of the possible connection of vanadium polyhedra in both [100] and [010] directions and so the two-dimensional character. It is reasonable to postulate that the core of the structure defined in (27) and (28) is present, some modulations occurring in order to adjust the chemical composition. The complexity of oxygen distribution is particularly emphasized by the difference Fourier section given in Fig. 6.

Type III: Solid Solution $Bi_4V_{2-z}Sb_zO_{11}$ ($z \leq 0.8$)

The formation of a solid solution by substitution of Sb^{5+} for V^{5+} in $Bi_4V_2O_{11}$ was reported by Joubert *et al.* (7). These

TABLE 2
Final Atomic Parameters for $Bi_{3.2}Sb_{0.8}V_2O_{10}$, $Bi_4V_2O_{10.5}$, and $Bi_4V_{1.2}Sb_{0.8}O_{11}$

Atom	Site	x	y	z	τ	$B_{eq}(*)_{or\ iso}$
			$Bi_{3.2}Sb_{0.8}V_2O_{10}$			
Bi	8g	0	0	0.3337(1)	0.8	2.00(8)*
Sb	8g	0	0	0.3166(5)	0.2	0.08(8)
V1	8e	0.041(2)	0	0	0.25	0.5(2)
V2	8f	0	0.052(3)	0	0.25	1.3(2)
O1	4e	1/4	1/4	1/4	1	1.8(5)
O2	4d	1/4	1/4	3/4	1	1.4(5)
O3	16k	0.279(8)	0.237(9)	0.022(2)	0.5	5.3(6)
O4	16k	0.021(9)	0.059(7)	0.107(3)	0.25	2.8(6)
			$Bi_4V_2O_{10.5}$			
Bi	8g	1/4	0.2319(4)	0.1689(1)	1	1.70(6)*
V1	8f	0.285(5)	0.679(4)	0	0.3	1.1(5)
V2	8f	0.291(6)	0.816(6)	0	0.2	1.0(6)
O1	16h	0.524(8)	−0.01(1)	0.746(3)	0.5	0.6(5)
O2	16h	0.45(2)	0.45(2)	0.01(1)	0.2	5(2)
O3	16h	0.56(2)	0.87(2)	− 0.03(1)	0.2	6(2)
O4	8f	0.37(2)	0.34(2)	0	0.2	2(1)
O5	8g	1/4	0.82(1)	−0.098(5)	0.625	2(1)
			$Bi_4V_{1.2}Sb_{0.8}O_{11}$			
Bi	8i	0	0	0.3296(4)	1	2.2(2)*
V/Sb	16o	0.023(9)	−0.01(3)	0	0.15/0.10	2.5(7)
O1	8f	1/4	1/4	1/4	1	1.3(7)
O2	32p	0.27(4)	0.21(4)	0.033(9)	0.25	6(4)
O3	32p	0.11(3)	0.05(3)	0.099(8)	0.1875	2(2)

authors suggested that the stabilization of different polymorphs of $Bi_4V_2O_{11}$ at room temperature depends on the doping level. The α and β phases, being modulated orthorhombic structures, are present up to $z = 0.15$ and $z = 0.30$, respectively. The upper limit for the γ-phase is $z = 1.0$ and the cell becomes tetragonal. In the same way, Joubert *et al.* performed a Rietveld refinement of two doped γ-$Bi_4V_{2-z}Sb_zO_{11}$ phases ($z = 0.5, 1$) in the $I4/mmm$ space group, taking as a starting model the structure of γ-$Bi_4V_2O_{11}$ (1) with a statistical distribution of Sb/V on the same crystallographic site around their ideal position as well as the oxygens of its layer.

In our study, we used different synthesis methods and found different results. The above authors used Sb_2O_3 as a starting product, the mixture being heated in air. This protocol could allow the partial oxidation of Sb^{3+} to Sb^{5+} transforming Sb_2O_3 into the Sb_2O_4 stable oxide. Then the possible formation of mixed doped phases in both Bi^{3+} and V^{5+} sites can occur, together with a small amount of Sb_2O_4 undetectable by X-ray diffraction methods. For this reason, we demonstrate the existence of a solid solution, $Bi_4V_{2-z}Sb_zO_{11}$, with a probable limit lower than $z = 1$; i.e., $z = 0.8$. The X-ray powder diffraction patterns (Fig. 2) show the existence of a single phase without peaks corresponding to superlattice reflections (γ-polymorph) until $z = 0.8$, while for $z = 1$ a mixture of γ phase and $BiSbO_4$ oxide is clearly present. On the other hand, the calculated unit-cell parameters from powder samples exhibit an increase of a and c and a decrease of b between $z = 0$ and $z = 0.2$ (Fig. 3III). For $0.2 \leq z \leq 0.8$, a and b decrease while c increases giving a very slight change in the lattice volume. Above $z = 0.8$ up to $z = 1$ no further evolution can be observed. Therefore, we can conclude that the maximum substitution for $Bi_4V_{2-z}Sb_zO_{11}$ solid solution corresponds to $z = 0.8$.

To elucidate the uncertainty derived from powder samples about the possible existence of superstructures and the space group of these phases, single crystals of the more highly substituted oxide $Bi_4V_{1.2}Sb_{0.8}O_{11}$ were grown.

The electron diffraction pattern (Fig. 4III) confirms the absence of superstructure spots and so the γ form of the $Bi_4V_{1.2}Sb_{0.8}O_{11}$ structure. Its structure has been deter-

TABLE 3
Selected Distances (Å) for $Bi_{3.2}Sb_{0.8}V_2O_{10}$, $Bi_4V_2O_{10.5}$, and $Bi_4V_{1.2}Sb_{0.8}O_{11}$

			$Bi_{3.2}Sb_{0.8}V_2O_{10}$		
Bi–O1	2.339(1) × 2		Sb–O1	2.202(4) × 2	
Bi–O2	2.339(1) × 2		Sb–O2	2.202(4) × 2	
Bi–O3	2.87(5)	3.08(5)	Sb–O3	3.08(5)	3.28(6)
Bi–O4	2.60(4)		Sb–O4	2.70(5)	
Bi … Sb[a]	0.27(1)				
V1 … V2[a]	0.36(1)	0.45(2)			
V1–O3	1.79(5)	1.88(5)	2.07(5)	2.21(5)	
V1–O4	1.70(5)	1.73(5)			
V2–O3	1.71(5)	1.87(5)	2.14(5)	2.23(5)	
V2–O4	1.67(5)	1.78(5)			
			$Bi_4V_2O_{10.5}$		
Bi–O1	2.19(1)	2.31(1)	2.41(1)	2.41(1)	
Bi–O2	2.91(2)				
Bi–O3	2.44(1)				
Bi–O4	2.74(2)				
V1 … V1[a]	0.39(2)				
V1 … V2[a]	0.76(2)	0.87(2)			
V2 … V2[a]	0.45(2)				
V1–O2	1.59(5)	1.63(9)	1.84(9)	1.98(9)	
V1–O3	1.91(9)	2.24(9)			
V1–O4	1.91(9)	1.95(9)	2.08(9)	2.30(9)	
V1–O5	1.70(8)	1.70(8)			
V2–O2	2.06(9)	2.23(9)	2.39(9)	2.45(9)	
V2–O3	1.60(9)	2.01(9)	2.03(9)	2.23(9)	
V2–O4	2.07(8)	2.48(8)			
V2–O5	1.52(8)				
			$Bi_4V_{1.2}Sb_{0.8}O_{11}$		
Bi–O1	2.309(3) × 4				
Bi–O2	2.775(3)				
Bi–O3	2.441(4)	2.770(3)			
V/Sb–O2	8 distance between 1.8(2) and 2.2(2)				
V/Sb–O3	4 distance between 1.7(1) and 1.8(1)				

[a] Distance intercrystallographic sites.

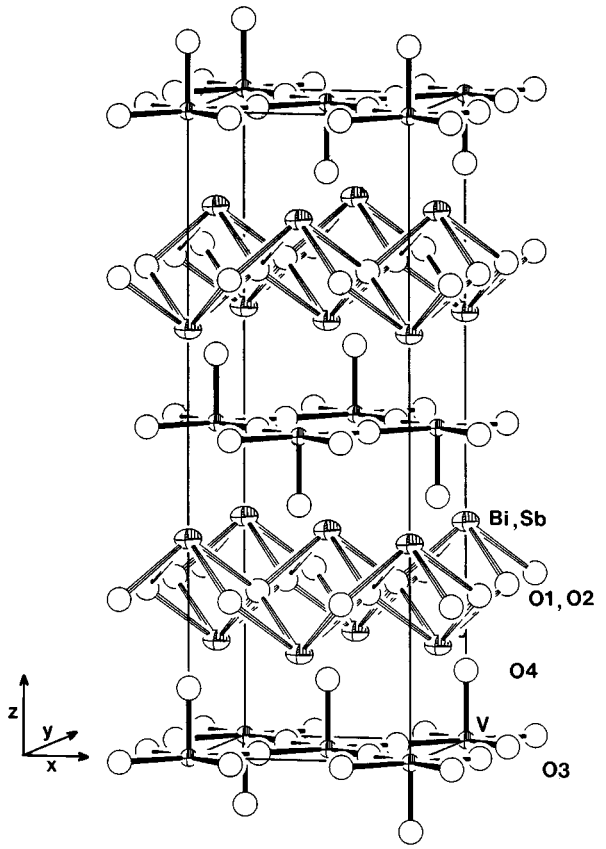

FIG. 5. View of the crystal structure of $Bi_{3.2}Sb_{0.8}V_2O_{10}$.

mined by X-ray single-crystal diffraction methods. The crystal data, atomic positions, and representative geometric parameters are listed in Tables 1, 2, and 3, respectively.

Accordingly to our results, $Bi_4V_{1.2}Sb_{0.8}O_{11}$ crystallizes in the orthorhombic system, space group *Fmmm* (No. 69) representing an average structure. Again $[Bi_2O_2]_n$ sheets and $[V_{1.2}Sb_{0.8}O_7]_n$ layers alternate within the framework, Sb^{5+} and V^{5+} occupying MO_6 octahedra, the remaining V^{5+} being inside distorted square pyramids. Figure 7 schematizes this idealized structure.

Comparison between $Bi_4V_2O_{10}$, $Bi_{3.2}Sb_{0.8}V_2O_{10}$, $Bi_4V_2O_{10.5}$, $Bi_4V_{1.2}Sb_{0.8}O_{11}$, and $Bi_4V_2O_{11}$ Structures

As has been described above, these five oxides retain the classical two-dimensional array with bismuth– or bismuth/antimony–oxygen layers alternating with vanadium– or vanadium/antimony–oxygen sheets. The latter contain more or fewer anionic vacancies, giving rise to different coordination polyhedra for vanadium, i.e. tetrahedra only for V^{5+}, square pyramids, distorted trigonal bipyramid, and octahedra for V^{4+} or V^{5+}, while antimony always exhibits octahedral coordination. Nonstoichiometry associated with ionic-conducting properties explains why some oxygen temperature factors have higher values.

The main crystallographic data are summarized in Table 4. The unit-cell parameters of these oxides are very close, but the variations can be reasonably interpreted:

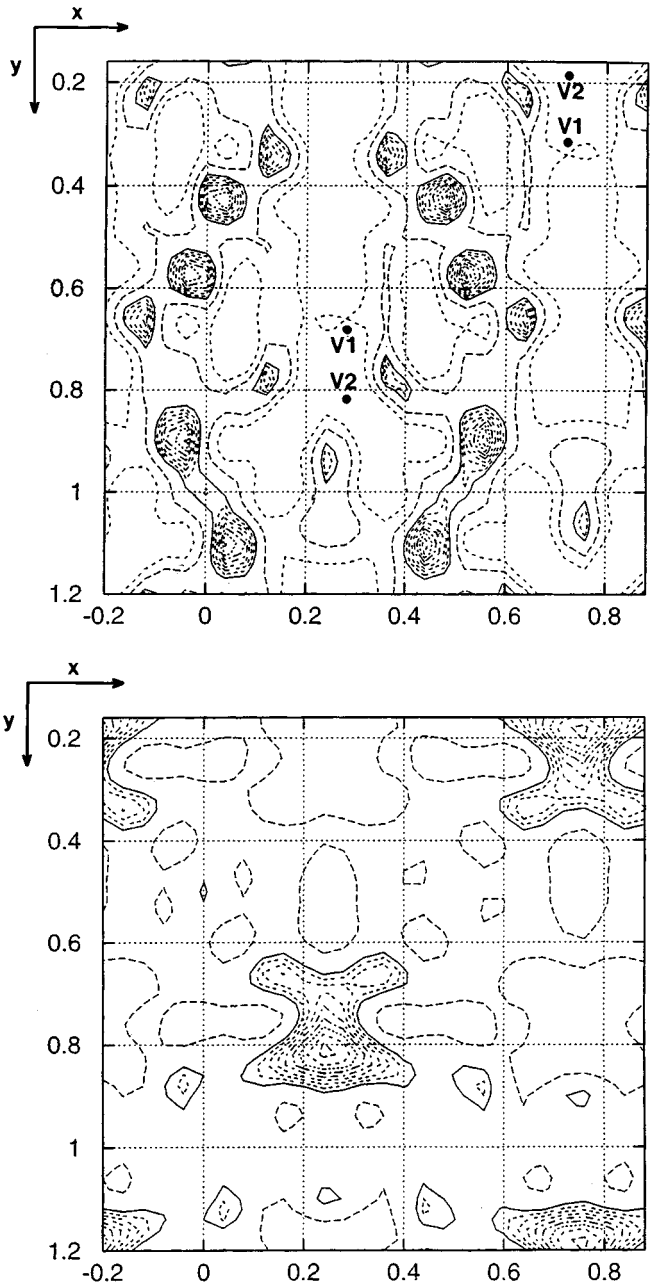

FIG. 6. Difference Fourier maps in the $Bi_4V_{1.2}Sb_{0.8}O_{11}$ structure: sections at $z = 0$ (up) and $z = -0.10$ (down) were computed with Bi, V1, V2, and O1 atoms. (The positions of V atoms are indicated by small dots. The most prominent peaks of the maps are assigned to disordered O atoms. The full lines correspond to 2.5 e $Å^{-3}$. The maxima correspond to 5.2 e $Å^{-3}$ for $z = 0$ and 7.1 e $Å^{-3}$ for $z = -0.10$, respectively).

TABLE 4
Comparisons of Cell Parameters of $Bi_4V_2O_{10}$, $Bi_{3.2}Sb_{0.8}V_2O_{10}$, $Bi_4V_2O_{10.5}$, $Bi_4V_{1.2}Sb_{0.8}O_{11}$, and $Bi_4V_2O_{11}$

	a (Å)	b (Å)	c (Å)	V (Å^3)	S.G.	Ref.
$Bi_4V_2O_{10}$	5.494(2)	5.505(3)	15.449(3)	467.2(2)	$P2_122_1$	10–11
$Bi_{3.2}Sb_{0.8}V_2O_{10}$	5.492(1)	5.493(1)	15.584(2)	470.1(2)	$F222$	This work
$Bi_4V_2O_{10.5}$	5.527(2)	5.574(1)	15.351(4)	472.9(2)	*Amam*	This work
$Bi_4V_{1.2}Sb_{0.8}O_{11}$	5.462(2)	5.469(2)	15.867(4)	474.0(2)	*Fmmm*	This work
$Bi_4V_2O_{11}$	$3 \times 5.528(3)$	5.594(2)	15.254(6)	$3 \times 471.5(4)$	*Pncm*	10

- In the $Bi_4V_2O_{10.5}$ phase, the c parameter is exactly midway between the c parameters of $Bi_4V_2O_{10}$ and $Bi_4V_2O_{11}$; this fact is in good agreement with statistical participation of both V^{4+} and V^{5+} cations.
- In the $Bi_{3.2}Sb_{0.8}V_2O_{10}$ phase containing Sb^{3+}, the c parameter increases in comparison with its value in the $Bi_4V_2O_{10}$ nonsubstituted phase. The increase is due to the repulsion effect of lone pairs associated with Sb^{3+} being more active than those associated with Bi^{3+}.
- In the $Bi_4V_{1.2}Sb_{0.8}O_{11}$ phase containing Sb^{5+}, the c parameter increases in comparison with the c parameter in the $Bi_4V_2O_{11}$ nonsubstituted phase. This fact is related to the different ionic radii: V^{5+} CN4 = 0.36 Å, CN5 = 0.46 Å, CN6 = 0.54 Å, and Sb^{5+} CN6 = 0.60 Å (23).

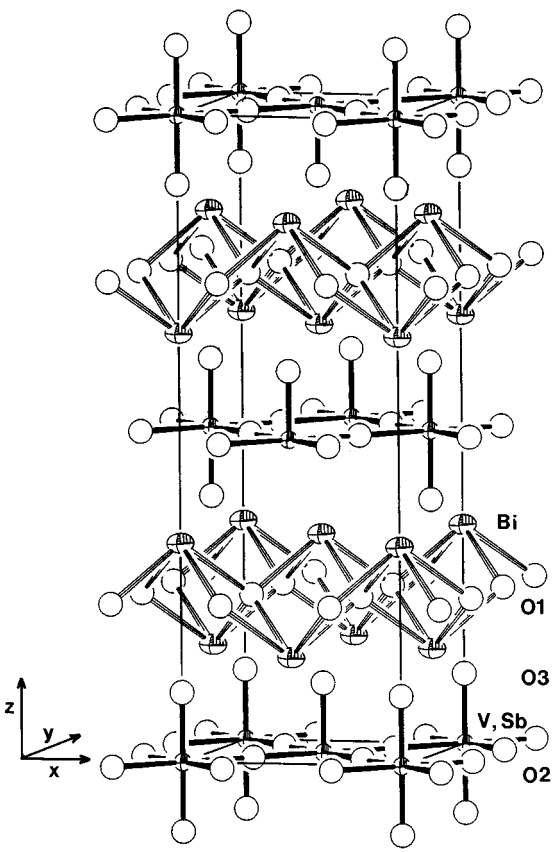

FIG. 7. Representation of the $Bi_4V_{1.2}Sb_{0.8}O_{11}$ structure.

Although the introduction of antimony into both $Bi_{3.2}Sb_{0.8}V_2O_{10}$ and $Bi_4V_{1.2}Sb_{0.8}O_{11}$ would seem equivalent, the degree of substitution evolves to 20% in the former and to 40% in the latter. This fact shows the different behavior of antimony Sb^{3+} and Sb^{5+} and the good control of the synthesis methods for the designed compounds. Moreover, while the $[Bi_2O_2]_n$ sheets remain stable for all studied compounds, the introduction of Sb^{3+} in that layer acts particularly on the vanadium–oxygen sheets, which can accommodate the various coordination polyhedra exhibited by V^{4+}, V^{5+}, and/or Sb^{5+}. This facility is undoubtedly the reason why these compounds are high ionic conductors.

This study presents another example of substitution of Sb for Bi in the $[Bi_2O_2]_n$ sheets of the Aurivillius structures. Moreover, the capability of $Bi_4V_2O_{10+\delta}$ ($0 \leq \delta \leq 1$) phases to accommodate composition and charge modifications, here shown, is obviously related to its exciting physical properties, such as ionic conductivity and ferroelectricity (29). For that reason, it can be postulated that these materials would be very good candidates to be used in several technical devices.

ACKNOWLEDGMENTS

The authors acknowledge the CNRS of France and CSIC of Spain for their joint project. A.C. and J.G. thank the financial supports of CICYT of Spain (Project MAT97-0711) and the Conseil Régional de Midi-Pyrénées (Project MAT 9609888), respectively.

REFERENCES

1. F. Abraham, J. C. Boivin, G. Mairesse, and G. Nowogrocki, *Solid State Ionics* **40/41,** 934 (1990).
2. T. Iharada, A. Hammouche, J. Fouletier, M. Kleitz, J. C. Boivin, and G. Mairesse, *Solid State Ionics* **48,** 257 (1991).
3. K. B. R. Varma, G. N. Subbanna, T. N. Guru Row, and C. N. R. Rao, *J. Mater. Res.* **5,** 2718 (1990).
4. C. K. Lee, B. H. Bay, and A. R. West, *J. Mater. Chem.* **6,** 331 (1996).
5. A. A. Bush and Yu. N. Venevtsev, *Russ. J. Inorg. Chem.* **31,** 769 (1986).
6. G. Mairesse, *Fast Ion Transp. Solids* 271 (1993).

7. O. Joubert, A. Jouanneaux, M. Ganne, R. N. Vannier, and G. Mairesse, *Solid State Ionics* **73,** 309 (1994).
8. H. R. Aghabozorg, W. R. Flavell, and B. H. Sakakini, *J. Catal.* **167,** 164 (1997).
9. O. Joubert, A. Jouanneaux, M. Ganne, and M. Tournoux, *Mater. Res. Bull.* **27,** 1235 (1992).
10. J. Galy, R. Enjalbert, P. Millán, and A. Castro, *C.R. Acad. Sci. Paris* **317-II,** 43 (1993).
11. S. Sorokina, R. Enjalbert, P. Baules, A. Castro, and J. Galy, *J. Solid State Chem.* **125,** 54 (1996).
12. P. Millán, J. M. Rojo, and A. Castro, *Bol. Soc. Esp. Ceram. Vidr.* **37,** 217 (1998).
13. A. Castro, P. Millán, M. J. Martínez-Lope, and J. B. Torrance, *Solid State Ionics* **63–65,** 897 (1993).
14. A. Castro, P. Millán, and R. Enjalbert, *Mater. Res. Bull.* **30,** 871 (1995).
15. P. Millán, A. Ramírez, and A. Castro, *J. Mater. Sci. Lett.* **14,** 1657 (1995).
16. A. Castro, P. Millán, R. Enjalbert, E. Snöeck, and J. Galy, *Mater. Res. Bull.* **29,** 871 (1994).
17. C. L. Ling, R. L. Withers, A. D. Rae, S. Schmid, and J. G. Thompson, *Acta Crystallogr.* **B52,** 610 (1996).
18. A. Ramírez, R. Enjalbert, J. M. Rojo, and A. Castro, *J. Solid State Chem.* **128,** 30 (1997).
19. A. C. T. North, D. C. Phillips, and F. S. Mattews, *Acta Crystallogr.* **A24,** 351 (1968).
20. D. T. Cromer and D. Liberman, "Internatonal Tables for X-Ray Crystallogrphy," Vol. IV. Kynoch Press, Birmingham, UK, 1974.
21. G. Sheldrick, "Program for Crystal Structure Determination, Version SHELX-86," Oxford Univ. Press, Cambridge, UK, 1986.
22. C. K. Johson, "Ortep II Report ORNL 5138," Oak Ridge National Laboratory, Oak Ridge, TN, 1976.
23. R. D. Shannon, *Acta Crystallogr.* **A32,** 751 (1976).
24. K. B. R. Varma and K. V. R. Prasad, *J. Mater. Res.* **11,** 2288 (1996).
25. J. B. Goodenough, A. Manthiram, M. Paranthanman, and Y. S. Zhen, *Mater. Sci. Eng.* **B12,** 357 (1992).
26. S. Lazure, R. N. Vannier, G. Nowogrocki, G. Mairesse, C. Muller, M. Anne, and P. Strobel, *J. Mater. Chem.* **5,** 1395 (1995).
27. O. Joubert, A. Joanneaux, and M. Ganne, *Nucl. Instrum. Methods, Phy. Res. Sect B.* **97,** 119 (1995).
28. M. Huve, R. N. Vannier, G. Nowogrocki, G. Mairesse, and G. Van Tendeloo, *J. Mater. Chem.* **6,** 1339 (1996).
29. K.V. R. Prasad and K. B. R. Varma, *Mater. Chem. Phy.* **38,** 406 (1994).